form a complex layer of $[(W_{11}O_{36})^{6-}]_\infty$ parallel to (001). There are large tunnels along **b** within the layers and Cs(3), Cs(4), Cs(5) and Cs(6) are located in them. Cs(1) and Cs(2) are located between the layers and connect neighbouring layers.

It is of interest to compare the structure of $Cs_6W_{11}O_{36}$ (W/Cs = 1·833) with that of $Cs_{22}W_{32}O_{107}$ (W/Cs = 1·455), which is isostructural with $Rb_{22}W_{32}O_{107}$ (Okada *et al.*, 1977), in order to examine the structural change accompanying the change in W/Cs ratio. The structure of $Cs_{22}W_{32}O_{107}$ is constructed by the three-dimensional framework of $[(W_{32}O_{107})^{22-}]_\infty$ built up of corner-shared W_4O_{18} groups. On the other hand, the structure of $Cs_6W_{11}O_{36}$ is constructed by complex layers of WO_6 octahedra by sharing corners. Apparently, there is little similarity between these two structures. However, W_4O_{18} groups are also observed in the $Cs_6W_{11}O_{36}$ structure, as shown in the area enclosed by dashed lines in Fig. 1. In fact, the complex layers in $Cs_6W_{11}O_{36}$ can be considered to be built up of W_4O_{18} groups. Accordingly, the three-dimensional framework of $[(W_{32}O_{107})^{22-}]_\infty$ changes to complex layers of $[(W_{11}O_{36})^{6-}]_\infty$ retaining the W_4O_{18} units, with increasing molar ratio W/Cs.

We are very grateful to Professor Y. Iitaka for his kindness in allowing us to use an automated four-circle diffractometer. Computations were carried out on HITAC 8700 and M-180 computers at the Computer Center of Tokyo Institute of Technology.

References

CHANG, L. L. Y. & SACHDEV, S. (1975). *J. Am. Ceram. Soc.* **58**, 267–270.

COPPENS, P. & HAMILTON, W. C. (1970). *Acta Cryst.* A**26**, 71–83.

HUGHES, E. W. (1941). *J. Am. Chem. Soc.* **63**, 1737–1752.

International Tables for X-ray Crystallography (1974). Vol. IV, pp. 71–151. Birmingham: Kynoch Press.

OKADA, K., MARUMO, F. & IWAI, S. (1977). *Acta Cryst.* B**33**, 3345–3349.

TOKONAMI, M. (1965). *Acta Cryst.* **19**, 486.

WUENSCH, B. J. & PREWITT, C. T. (1965). *Z. Kristallogr.* **122**, 24–59.

Acta Cryst. (1978). B**34**, 54–63

Refinement of the Molecular Charge Distribution in Decaborane(14)

BY HANS DIETRICH AND CHRISTIAN SCHERINGER*

Fritz-Haber-Institut der Max-Planck-Gesellschaft, 1000 Berlin-Dahlem, Federal Republic of Germany

(*Received* 15 *November* 1976; *accepted* 24 *July* 1977)

The model published by Brill, Dietrich & Dierks [*Acta Cryst.* (1971), B**27**, 2003–2018] has been further developed and refined by least-squares methods after improving the data reduction of the original measurements. The diffuse charge density spread within the boron framework of the molecule has been accounted for in two different ways, yielding about the same total description of the molecular charge distribution. $F_o - F_c$ syntheses do not indicate further amendments and show only deviations due to errors in the measurements. Elimination of the thermal smearing from the models allows the calculation of the static difference density $(M - A)$ between the molecular charge distribution and isolated atoms, which can be compared directly with quantum-chemical calculations. The comparison shows good agreement in some respects, disagreement in others.

Introduction

It is well known that localized bonds and lone pairs of electrons cause broad diffuse peaks in $X - N$ syntheses, very similar to peaks in $F_o - F_c$ syntheses, from which the positions of hydrogen atoms are derived in a structure determination. This may justify the attempt to approximate these peaks by smeared point charges and treating them in a similar way to light atoms. On the other hand, the corresponding charge must come from the atoms within the molecule, and therefore it would no longer be correct to treat the atoms as electrically neutral.

Based on these considerations, Brill, Dietrich & Dierks (1971) – hereinafter referred to as BDD – proposed a purely empirical model, which approximates the total molecular electron density by a superposition of spherical atomic cores and smeared point charges. BDD's model (model I in this paper) was refined with trial-and-error and Fourier methods and was subject to a number of restrictions. It contained only 15 density parameters.

* New address: Fachbereich Geowissenschaften der Universität Marburg, Lahnberge, 3550 Marburg, Federal Republic of Germany.

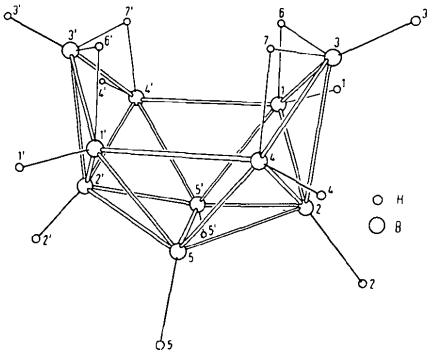

Fig. 1. Molecular structure of $B_{10}H_{14}$.

In the present work these restrictions are partially released. Our improved models are described by a maximum of three positional parameters, anisotropic smearing for the introduced point charges, and by linear constraints among the parameters (chemical symmetry). The diffuse density in the boron framework is approximated in three different ways: models II, III and IV with 55, 54 and 68 density parameters respectively. Model IV, though given in Fig. 2, will not be discussed much further since its refinement presented difficulties.

The refinements are carried out by means of full-matrix least squares based on F. $F_o - F_c$ syntheses are used to check the resulting models for systematic errors.

Since the thermal smearing functions (vibration tensors) are defined separately for each density unit of our models, it is straightforward to eliminate the thermal parameters from the models and to calculate the density for the molecule at rest. This makes possible a direct comparison of our results with the quantum-chemical results obtained by Laws, Stevens & Lipscomb (1972*a*).

For our new approach the data reduction of the X-ray measurements is improved, including the absorption correction for the glass capillary (Dierks & Dietrich, 1968), in which the crystal was sealed. A unique set of 1577 data is obtained. The positional and thermal parameters are the same as those derived by BDD from the neutron diffraction data of Tippe & Hamilton (1969). The molecular structure of decaborane(14) is shown in Fig. 1.

Definition of the parameters for the refinement

In order to facilitate the utilization of local symmetry and chemical equivalence, it is convenient to express the parameters of each point charge in terms of a special reference system defined only by the neighbouring atoms within the molecule.

Generally, one of the neighbouring atoms of each point charge is selected as the main reference atom A_1, in which the origin of a Cartesian coordinate system **Y** is placed. The direction of the axis Y_3 is chosen so that it passes through a weighted mean of the positions of the atoms A_2, $A_3 \ldots A_n$, partaking in an n-centre bond together with A_1. The weighted mean expressed in crystal coordinates is

$$\mathbf{x}_m = \sum_{i=2}^{n} \frac{\mathbf{x}(A_1)}{d(A_1A_i)} \Big/ \sum_{i=2}^{n} \frac{1}{d(A_1A_i)} \qquad (1)$$

where $d(A_1A_i)$ is the distance between the atoms A_1 and A_i. In Fig. 2, which represents a schematic drawing of the four models, the positive directions of the Y_3 axes are marked by arrows beginning at the reference atoms A_1.

For a point charge approximating the excess charge in a normal two-centre bond, which should have rotational symmetry, the two axes Y_2 and Y_1 are equivalent and their directions need not be fixed in space.

If the two-centre bond is bent, the rotational symmetry is lowered to m. In this case, an additional reference atom A_R is needed to define the plane in which the bond is bent. Then Y_2 is chosen to lie in this plane, with its positive direction pointing away from A_R. The axis Y_1 is then normal to the plane, but its direction is irrelevant, because of the symmetry m.

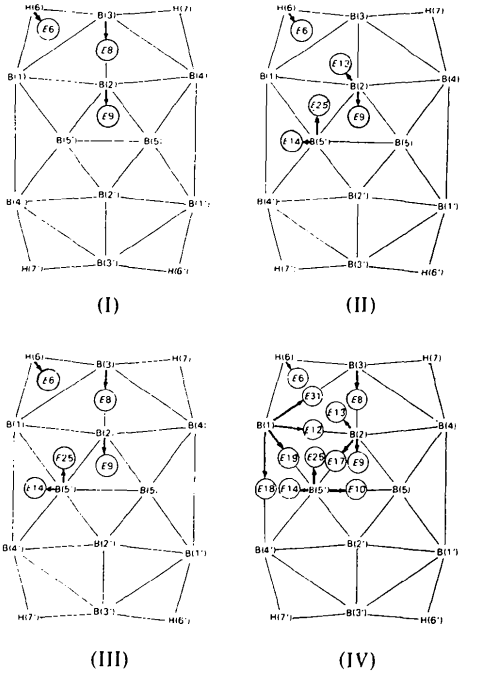

Fig. 2. Charts of the framework of $B_{10}H_{14}$ including the bridge H atoms and point charges (E) introduced in the framework in models I, II, III and IV. The terminal H atoms are left out.

For a point charge used to approximate the excess density in a three-centre bond, the axis Y_2 is chosen to be in the plane of the three atoms $A_1A_2A_3$, its positive direction pointing towards A_2. If the three-centre bond has m symmetry, the direction of Y_1, which is perpendicular to the plane, is again irrelevant. Otherwise an additional reference atom A_R is required, and the positive direction of Y_1 is then chosen to point away from A_R. So the system **Y** may be left-handed or right-handed depending on the local configuration of the neighbouring atoms.

As the intramolecular coordinate systems **Y** are chosen to correspond to the local approximate chemical symmetry, they can be used as the axis systems of smearing ellipsoids for the point charges. If pure Gaussian smearing is assumed, the normalized smearing function for the point **Y** is

$$\rho(\mathbf{Y}) = (2\pi)^{-3/2}(V_{11}V_{22}V_{33})^{-1/2} \times \exp\left(-\frac{1}{2}\left\{\frac{[Y_1 - Y_1(E)]^2}{V_{11}} + \frac{[Y_2 - Y_2(E)]^2}{V_{22}} + \frac{[Y_3 - Y_3(E)]^2}{V_{33}}\right\}\right). \quad (2)$$

V_{11}, V_{22}, V_{33} are the diagonal elements of a smearing tensor the off-diagonal terms of which should be approximately zero. The Fourier transform of the smearing function (2) in the system **Y** is

$$g(S_1S_2S_3) = \exp[-2\pi^2(S_1^2V_{11} + S_2^2V_{22} + S_3^2V_{33})] \quad (2a)$$

or, based on the crystal axes,

$$g(hkl) = \exp[-2\pi^2(h^2v_{11} + k^2v_{22} + l^2v_{33} + 2hkv_{12} + 2hlv_{13} + 2klv_{23})], \quad (2b)$$

where hkl are the Miller indices and v_{ij} are the transformed components of the smearing tensor. The function g represents an anisotropic form factor for a point charge normalized to the charge of one electron, $q = -1$.

Since each point charge possesses a maximum of seven parameters (**Y**, q, V_{11}, V_{22}, V_{33}), and each atomic core one parameter (q), models II and III would produce a maximum of 220 and 206 density parameters, respectively, in the asymmetric unit. Clearly, these are too many for a refinement, and we have reduced the number of parameters by means of constraints to 55 and 54 respectively. The 'equal molecule'-constraint is applied to the two half molecules in the asymmetric unit. Further constraints within the molecule ('equal-bond' constraints, rotational symmetry of bonds) are indicated in Tables 1 and 2 for models II and III respectively.

The thermal parameters $\mathbf{U}(E)$ of the point charge E, introduced for the approximation of the excess charge in an n-centre bond were interpolated according to

$$\mathbf{U}(E) = \sum_{i=1}^{n} \frac{1}{d(EA_i)}\mathbf{U}(A_i) \Big/ \sum_{i=1}^{n} \frac{1}{d(EA_i)} \quad (3)$$

where $d(EA_i)$ is the distance between E and the atom A_i partaking in the bond. $U(A_i)$ are the thermal parameters of the nucleus of A_i as determined from the

Table 1. *Parameters of model* II

The estimated standard deviations in terms of the last decimal place are given in parentheses. Number of parameters: 55. R_I = 0·0497, dipole moments: molecule 1 6·00 D, molecule 2 6·04 D.

	Definition of **Y**				Charge	Position (Å)			Smearing (Å²)		
Centre	A_1	A_2	A_3	A_R	q	Y_1	Y_2	Y_3	$2\pi^2V_{11}$	$2\pi^2V_{22}$	$2\pi^2V_{33}$
B(1)	B(1)				1·00 (30)						
B(2)	B(2)				1·47 (37)						
B(3)	B(3)				0·86 (25)						
B(5′)	B(5′)				as B(2)						
H(1)	H(1)				0·14 (18)						
H(2)	H(2)				−0·00 (45)						
H(3)	H(3)				0·14 (21)						
H(5′)	H(5′)				as H(2)						
H(6)	H(6)				0·34 (7)						
*E*1	H(1)	B(1)			−0·52 (6)	0·00	0·00	0·45 (2)	2·2 (2)	as V_{11}	2·6 (3)
*E*2	H(2)	B(2)			−0·57 (8)	0·00	0·00	0·48 (2)	2·6 (3)	as V_{11}	2·3 (3)
*E*3	H(3)	B(3)			−0·54 (8)	0·00	0·00	0·48 (3)	2·6 (3)	as V_{11}	2·4 (4)
*E*5′	H(5′)	B(5′)			as *E*2						
*E*6	H(6)	B(1)	B(3)		−0·45 (8)	0·00	0·00	0·42 (3)	2·6 (4)	3·0 (6)	2·3 (4)
*E*9	B(2)	B(5′)	B(5)	B(3)	−0·34 (12)	0·12 (4)	0·00	1·08 (5)	2·3 (6)	2·9 (11)	2·4 (7)
*E*13	B(2)	B(3)	B(1)	B(4)	−0·18 (3)	0·01 (2)	0·34 (6)	1·02 (5)	1·1 (3)	2·8 (13)	1·7 (5)
*E*25	B(5′)	B(1)	B(2)	B(1′)	−0·95 (32)	0·05 (3)	−0·07 (8)	1·24 (11)	3·1 (5)	5·6 (15)	9·2 (20)
*E*14	B(5′)	B(4′)	B(1)	B(5)	−0·63 (26)	0·01 (3)	0·00	1·19 (14)	2·6 (6)	6·7 (32)	5·9 (19)
*E*20	H(6)	H(7′)	B(5′)		−0·06 (4)	0·00	0·00	1·00	1·5 (23)	4·4 (54)	1·0 (16)

Table 2. *Parameters of model* III

The estimated standard deviations in terms of the last decimal place are given in parentheses. Number of parameters: 54. $R_F = 0.0504$, dipole moments: molecule 1 6·66 D, molecule 2 6·69 D.

	Definition of **Y**				Charge	Position (Å)			Smearing (Å^3)		
Centre	A_1	A_2	A_3	A_R	q	Y_1	Y_2	Y_3	$2\pi^2 V_{11}$	$2\pi^2 V_{22}$	$2\pi^2 V_{33}$
B(1)	B(1)				1·38 (34)						
B(2)	B(2)				1·31 (32)						
B(3)	B(3)				1·22 (34)						
B(5′)	B(5′)				as B(2)						
H(1)	H(1)				0·17 (17)						
H(2)	H(2)				0·04 (26)						
H(3)	H(3)				0·14 (23)						
H(5′)	H(5′)				as H(2)						
H(6)	H(6)				0·31 (7)						
*E*1	H(1)	B(1)			−0·56 (6)	0·00	0·00	0·44 (2)	2·3 (2)	as V_{11}	2·5 (3)
*E*2	H(2)	B(2)			−0·62 (8)	0·00	0·00	0·52 (2)	2·5 (3)	as V_{11}	2·7 (3)
*E*3	H(3)	B(3)			−0·66 (10)	0·00	0·00	0·51 (3)	2·9 (4)	as V_{11}	2·7 (4)
*E*5′	H(5′)	B(5′)			as *E*2						
*E*6	H(6)	B(1)	B(3)		−0·52 (8)	0·00	0·00	0·40 (2)	2·6 (3)	3·7 (6)	2·0 (4)
*E*8	B(3)	B(2)		B(3′)	−1·02 (20)	0·00	−0·09 (2)	0·77 (5)	8·7 (15)	2·7 (4)	3·4 (7)
*E*9	B(2)	B(5′)	B(5)	B(3)	−0·34 (11)	0·13 (3)	0·00	1·13 (6)	2·2 (6)	2·6 (10)	2·2 (7)
*E*25	B(5′)	B(1)	B(2)	B(1′)	−0·53 (17)	0·06 (3)	−0·15 (7)	0·99 (7)	2·5 (4)	4·3 (10)	4·1 (13)
*E*14	B(5′)	B(4′)	B(1)	B(5)	−1·20 (38)	0·01 (3)	0·00	1·19 (10)	3·2 (6)	15·4 (48)	6·4 (15)
*E*20	H(6)	H(7′)	B(5′)		−0·06 (4)	0·00	0·00	1·00	1·0 (14)	7·5 (78)	1·0 (14)

neutron diffraction data. (3) gives vibration tensors which are somewhat too large, but this will impair the results of the electron density distribution only within the limits of error (Scheringer, 1977*a*,*b*).

Structure-factor calculation and refinement procedure

For the structure-factor calculation it is convenient to add the chemical-smearing tensor $\mathbf{v}(E)$ to the interpolated vibration tensor $\mathbf{U}(E)$, so that the chemical smearing of the point charge E is included in the temperature factor. Formally, this leaves just the charge $q(E)$ for the scattering factor of E, which can be treated as an occupancy factor, except for the sign

$$f(E) = -q(E). \tag{4}$$

In principle, the sign of q may also be positive, and that of f negative. In this case the purpose of point charge E is to approximate a deficiency instead of an excess of electron density.

For the refinement of the atomic cores, BDD had used linear interpolation between the scattering curves of B, B^{1+}, B^{2+}, H, and H^{1-} published in *International Tables for X-ray Crystallography* (1962). In our present study, we employed the *L*-shell projection method of Stewart (1970) for the B cores, and used linear interpolation between scattering curves of H^{1-}, H, $H^{0.25+}$, and $H^{0.5+}$. The latter two curves were obtained according to Dietrich (1976*a*).* Accurate logarithmic interpolation of the scattering curves (Dietrich, 1976*b*) was used throughout.

As the positional and the smearing parameters of the point charges were chosen in the special intramolecular coordinate systems **Y**, the transformations between these systems and the crystallographic coordinate system had to be worked out. This was done in several steps. First we transformed the crystal coordinates of the atoms to a standard Cartesian reference system. Then its origin was shifted into that of the system **Y**, and the axes rotated to coincide with those of **Y**. For the total transformation **G** we have

$$\mathbf{Y} = \mathbf{G}\mathbf{x} + \mathbf{Y}_o, \quad \mathbf{x} = \mathbf{G}^{-1}\mathbf{Y} + \mathbf{x}_o \tag{5}$$

where $\mathbf{Y}_o$ and $\mathbf{x}_o$ indicate the appropriate shifts of the origin. For the transformations of the smearing tensor we obtain

$$\mathbf{V} = \mathbf{G}\mathbf{v}\mathbf{G}^T, \quad \mathbf{v} = \mathbf{G}^{-1}\mathbf{V}\mathbf{G}^{T-1}, \tag{6}$$

where T denotes the transposed matrix.

The derivatives of the structure factor F with respect to **Y** and **V** are

$$\frac{\partial F}{\partial \mathbf{Y}} = \mathbf{G}^{T-1}\frac{\partial F}{\partial \mathbf{x}} \tag{7}$$

and

$$\frac{\partial F}{\partial \mathbf{V}} = \mathbf{G}^{T-1}\frac{\partial F}{\partial \mathbf{v}}\mathbf{G}^{-1} \tag{8}$$

respectively. The derivatives (7) and (8) were computed analytically. The possible constraints were treated essentially according to Busing (1971), whereby numerical differentiation was partly employed. The calculation of the derivatives for constraint parameters

* Fig. 11 shows that this approximation should be good enough, *i.e.* the difference density in the vicinity of the proton is mainly due to the bond peak.

has been described by Scheringer (1965*b*), Pawley (1972), and Raymond (1972). The restriction imposed on the charges by the condition that the total electric charge within the cell must be zero would normally be allowed for by setting one of the charges equal to the negative sum of all the other charges. In the present case, however, this procedure cannot be applied, since the calculated shifts are too large and have to be reduced by damping factors. Therefore we computed shifts for all charges q and distributed the negative equivalent of the total excess charge equally on all of them in each cycle of refinement. It is not important how the excess charge is distributed on the charge parameters q, as long as none of them is excluded, since the excess charge built up in each cycle is much smaller than the shifts in the same cycle.

Considerable damping of the parameter shifts was necessary at the beginning of the refinements. At the end the computed shifts became, as usual, small compared with the estimated standard deviations. There were some exceptions with the parameters describing the diffuse electron density within the boron skeleton. The inherent difficulties will be discussed in the following section.

Treatment of the smoothly spread density within the boron framework (Fig. 3)

This can be done in several ways, and therefore we have worked out three models, II, III and IV, differing with respect to the number and arrangement of density ellipsoids employed (Fig. 2). Since the description of the localized bonds, especially in the terminal B–H groups is the same in all models, the terminal hydrogens are not included in the schemes.

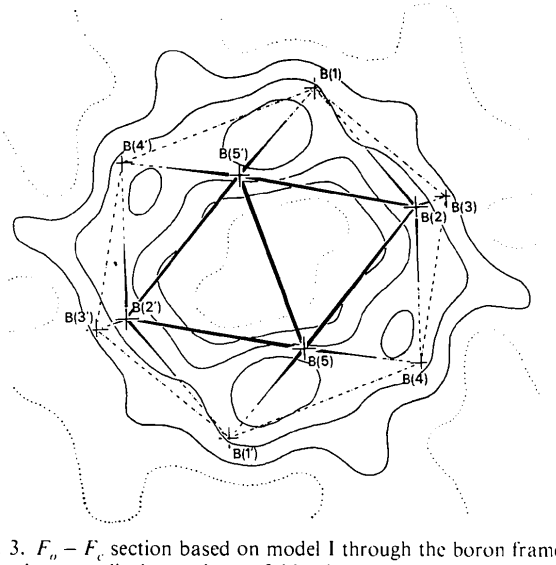

Fig. 3. $F_o - F_c$ section based on model I through the boron framework perpendicular to the twofold axis (BDD). Contour interval 0·1 e Å^{-3}, zero contour dotted.

In model II we put one point charge in each boron triangle. During refinement the localized bond between B(2) and B(3) documented itself by a shift of the point charge $E13$ and its chemical equivalent in the adjacent quadrant of the molecule towards the line B(2)–B(3), where the two ellipsoids overlap to give a diffuse peak. A similar peak is obtained by replacing $E13$ and its chemical equivalent by a long flat ellipsoid with its long axis perpendicular to the line B(2)–B(3). This consideration led to the point charge $E8$ in model III. Furthermore, the $F_o - F_c$ synthesis indicated the need to insert a small charge on the line H(6)–H(7′) for both models II and III. This charge is labelled $E20$, and, though not indicated in Fig. 2, its parameters will be given in the Tables 1 and 2.

Finally, we obtained model IV from model II by placing additional scattering centres on all B–B edges of the boron framework.

In general, one would expect that the diffuse electron density within the boron framework can be approximated better if more ellipsoids are used. There are, however, limits set by the data and by the least-squares method. Regarding the latter, the matrix increases rapidly in size with the number of parameters and tends to become ill-conditioned, because the correlation between charge and smearing parameters of neighbouring point charges becomes more serious when their distances decrease and their overlap increases. Then the least-squares fitting process becomes very sensitive to errors in the data and is left unstable with too large shifts (Scheringer, 1965*a*). This consideration led to the exclusion of model IV from the present work.

On the other hand, the use of constraints reduces the number of parameters and thereby stabilizes the refinement effectively. We believe that, with the constraints employed in models II and III, a good compromise was reached so as to stabilize the refinement on the one hand, and, on the other, to allow sufficient flexibility for distributing the density in the molecule.

Results of the refinement

The results of the refinements for models II and III are summarized in Tables 1 and 2 respectively. The constraints applied are also indicated in the tables. The thermal parameters are not given, since they can easily be calculated from (3) and the nuclear parameters derived by BDD.

The R values for models II and III are 0·0497 and 0·0504 respectively for the complete set of data (no 'less thans'). (For BDD's model I the R value is 0·0692.) The $F_o - F_c$ syntheses (see Fig. 6) indicate that the refinements were complete. The sections referring to chemically equivalent (but crystallographically independent) regions clearly have no common features. This proves that the deviations left are not

caused by insufficiencies of the model, but must be due to the errors in the data. (The largest deviations from zero found were +0·25 and −0·3 e Å^{-3}.)

The standard deviations given in the tables were calculated from the inverse matrix of the full set of parameters, and they are large. We do not consider this to be serious, since this is only a consequence of the fact that a fair number of correlated parameters is needed to allow an appropriate description of the density distribution in the molecule. (There is overlap between the charges of the atomic cores and the charges of the ellipsoids, and there is also correlation of the charges with the shape parameters of the ellipsoids.)

We calculated the estimated standard deviation of the difference density by applying Rees's (1976) equations (1) and (10). We put $\sigma(\rho_c) = 0$. Also the scale factor term, even with $\sigma(k)/k$ as large as 0·01, gave a negligible contribution. The main term is $\sigma(\rho_o)/k$. Calculation of this term leads to $\sigma(\Delta\rho) = 0{\cdot}044$ e Å^{-3}.

The charges of the 'hydrogen cores' show a tendency to become slightly positive, but the values are not significantly different from zero, except those of the bridge hydrogen atoms, H(6) and its equivalents. For these, positive charges of 0·34 and 0·31 were obtained for models II and III respectively.

The approximation of the density distribution within the terminal B–H groups is the same for the two models within the limits of error. The smearing of the excess charges in these localized B–H two-centre bonds appears to be nearly isotropic. It is not surprising that the amount of excess charge needed depends a little on the charge of the B core involved. This is especially obvious from $E3$. The charge found for the B(3) core is influenced by the way in which the asymmetrical bond B(2)–B(3) and the diffuse density within the two adjacent boron triangles is approximated.

Both models II and III suggest some charge between the atoms B(1) and B(4′), although the distance between these atoms is about 0·2 Å longer than all other B–B distances within the boron framework. The charge transfer is effected by the large values of the parameters q, Y_3, and V_{33} of $E14$, the only point charge available in that region. The elongation of the ellipsoid parallel to B(1)–B(4′) (large V_{22}) supplies charge between the atoms B(1)–B(5′) and the equivalent region B(4)–B(5′).

The representation of the localized bond B(2)–B(3) in model II (Table 1) by the point charge $E13$ and its equivalent beyond B(2)–B(3) requires a large parameter Y_2 of $E13$, *i.e.* a shift towards B(2)–B(3). On the other hand, the centre $E8$ in model III (Table 2) has also to account for the diffuse density in the boron triangles B(1)B(2)B(3) and B(4)B(2)B(3). Since the planes of these triangles form considerable angles with each other, it could be expected that $E8$ would shift a little off the line B(2)–B(3) towards the centre of the molecule. Therefore, $E8$ has been introduced in model III as a 'bent bond'. As expected, it was shifted slightly inside the framework which is seen from the negative value of Y_2. The charge in the triangle B(1)B(2)B(3) and its equivalent is distributed by means of the large parameters q and V_{11} of $E8$.

There is a remarkable difference in the charges of $E14$ in models II (q = 0·63 e) and III (q = 1·20 e). The reason is that, in model III, $E14$ is highly extended in the Y_2 direction and supplies diffuse density in the region around $B1$, whereas in model II this density is mainly supplied from $E13$ and $E25$, and to a smaller extent from $E14$.

It is somewhat surprising that the three-centre charge $E9$ is not a flat ellipsoid, either in model II or in model III, whereas $E25$ and $E14$ display a flat charge distribution.

From Tables 1 and 2 it can be seen that the parameters Y_1 of the three-centre charges introduced into the boron framework are generally small positive values. This means that these three-centre ellipsoids are situated slightly outside the planes of the boron framework.

Comparison with quantum-chemically calculated density distributions

The density distribution in the decaborane molecule was calculated quantum-chemically by Laws, Stevens & Lipscomb (1972*a*) – hereinafter referred to as LSL – (SCF calculation with a minimum basis). Furthermore, a very accurate calculation of the density

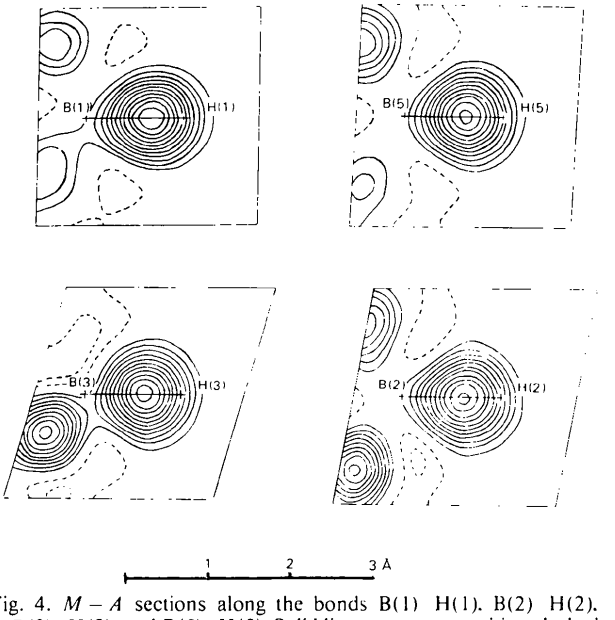

Fig. 4. $M-A$ sections along the bonds B(1) H(1), B(2) H(2), B(3)–H(3), and B(5)–H(5). Solid lines represent positive, dashed lines negative, contours. The contour interval is 0·05 e Å^{-3}. The zero contours have been omitted to show more clearly the deviations from zero in the sections.

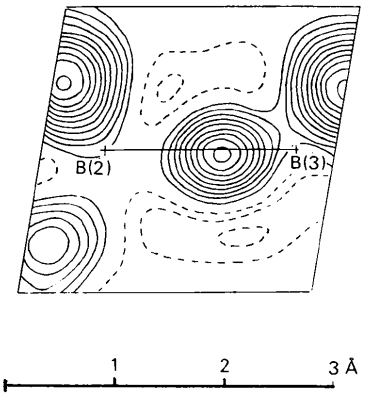

Fig. 5. $M-A$ section along the molecular mirror plane passing through the atoms B(2) and B(3). Contours as in Fig. 4.

distribution in the B–H radical was performed by Bader, Keaveny & Cade (1967). In the following we will compare our densities, obtained by experiment, with those calculated quantum-chemically. For this purpose we represent the results of our refinement by Fourier syntheses of the density. Since quantum-chemical calculations give the density for the molecule at rest, we eliminated the thermal smearing from our models and calculated the Fourier synthesis of the difference density ρ (molecule at rest) $-$ ρ (isolated atoms at rest), hereinafter referred to as an $M-A$ map. The elimination of the thermal parameters is performed by putting the vibration tensor for each density unit equal to zero in the expression for the structure factor. Then, the structure factors so obtained are used to calculate the $M-A$ maps. The $M-A$ maps given in Figs. 4 to 9 are based on model II (model III gave nearly identical results).

In the Fourier representation of the static density distribution ($M-A$ map) we restricted ourselves only to those details which can be determined from the experimental data. Thus, we used Fourier coefficients at the reciprocal-lattice points of the crystal and terminated the series at the experimental limit, $[(\sin\theta/\lambda)_{max} = 0{\cdot}62$ Å $^{-1}]$. This gives rise to a series-termination error in the $M-A$ maps, Figs. 4 to 9. The series termination will essentially lower the density at the centres of sharp peaks. A quantitative estimate after Scheringer (1977*c*) shows that the decrease in height of the steepest peaks in our $M-A$ maps, the terminal B–H bond peaks, amounts to about 0·1–0·2 e Å^{-3}, and should be less than 0·1 Å^{-3} for the other peaks.

The errors in the $M-A$ maps are estimated from the standard deviations of the F_o-F_c synthesis. Except for the effect of series termination discussed above, the standard deviation is 0·05 e Å $^{-3}$. Because of twofold or

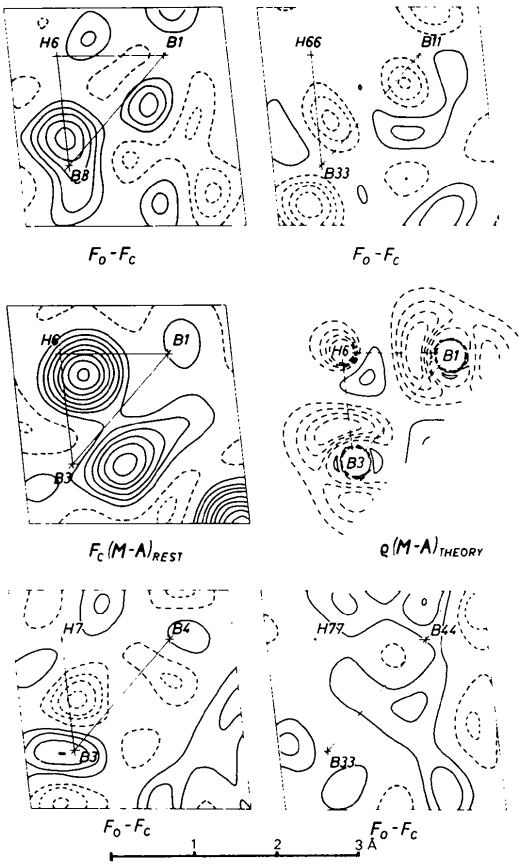

Fig. 6. Experimental (left) and theoretical (right, SCF after LSL) $M-A$ sections and corresponding F_o-F_c sections in the plane B(1)–H(6)–B(3). In the theoretical map the numbering of atoms has been changed to that used in this paper. Contours as in Fig. 4.

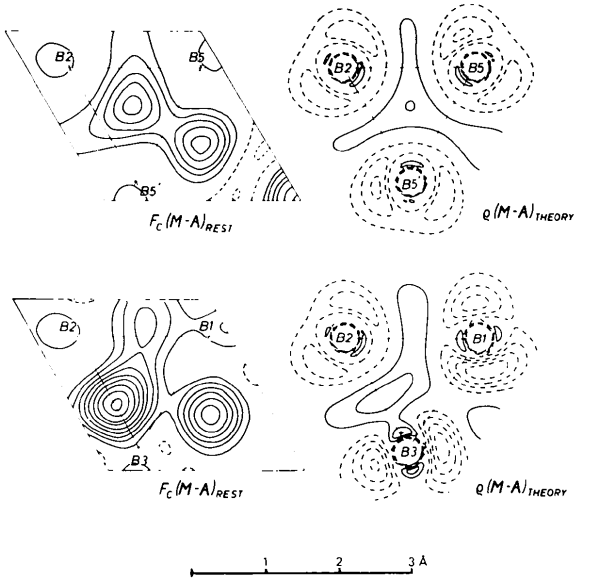

Fig. 7. Experimental (left) and theoretical (right, SCF after LSL) $M-A$ sections in the planes B(2)–B(5)–B(5′) and B(1)–B(2)–B(3). In the theoretical maps the numbering of atoms has been changed to that used in this paper. Contours as in Fig. 4.

fourfold chemical symmetry, the errors are reduced by factors of 0·71 and 0·50 respectively. Close to the nuclei the errors in the $M-A$ maps are certainly larger because the nuclear cusps cannot be observed with X-ray data and thus do not occur in our $M-A$ maps.

Our $M-A$ maps are reproduced in Figs. 4–9, together with the density sections calculated by LSL (Figs. 6–8; on the left is our section, on the right the corresponding one by LSL). LSL's numbering of the atoms has been changed to match ours in order to facilitate the comparison. All contour intervals are 0·05 e Å^{-3} and the zero contours are omitted. Fig. 10 shows LSL's calculation for the line along the B(2)–H(2) bond. Our experimental $M-A$ curve is inserted as a dashed line.

For the terminal B(2)–H(2) bond (Fig. 10) LSL find the maximum of the diffuse peak on the bond axis

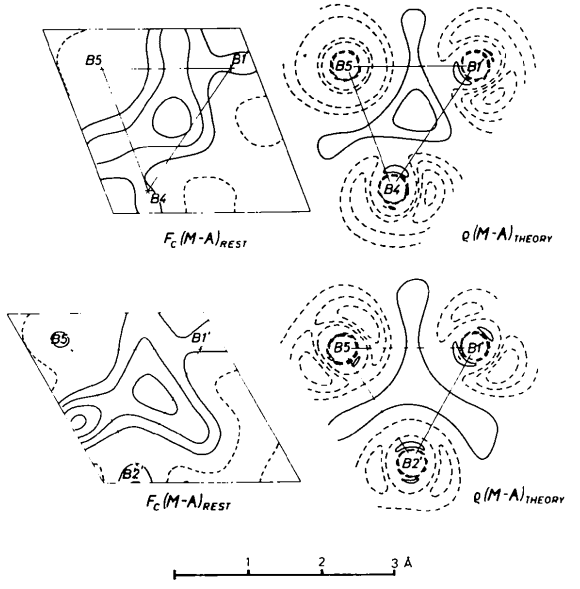

Fig. 8. Experimental (left) and theoretical (right, SCF after LSL) $M-A$ sections in the plane B(4)–B(5)–B(1′) [or its equivalent B(1)–B(5′)–B(4′)] and in the plane B(2′)–B(5)–B(1′) [or its equivalent B(2)–B(5′)–B(1)]. In the theoretical maps the numbering of atoms has been changed to that used in this paper. Contours as in Fig. 4.

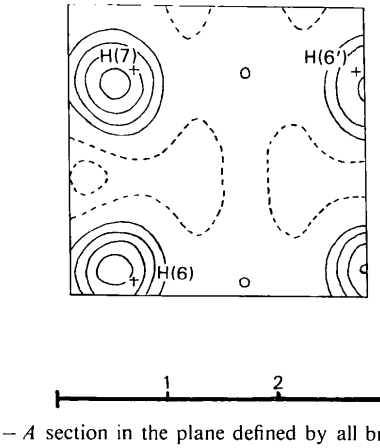

Fig. 9. $M-A$ section in the plane defined by all bridge H atoms. Contours as in Fig. 4.

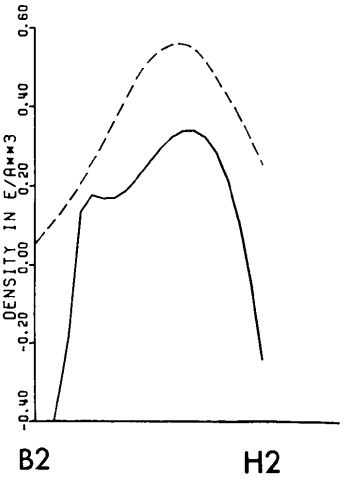

Fig. 10. Theoretical (after LSL, full line) and experimental (dashed) $M-A$ density along the bond B(2)–H(2).

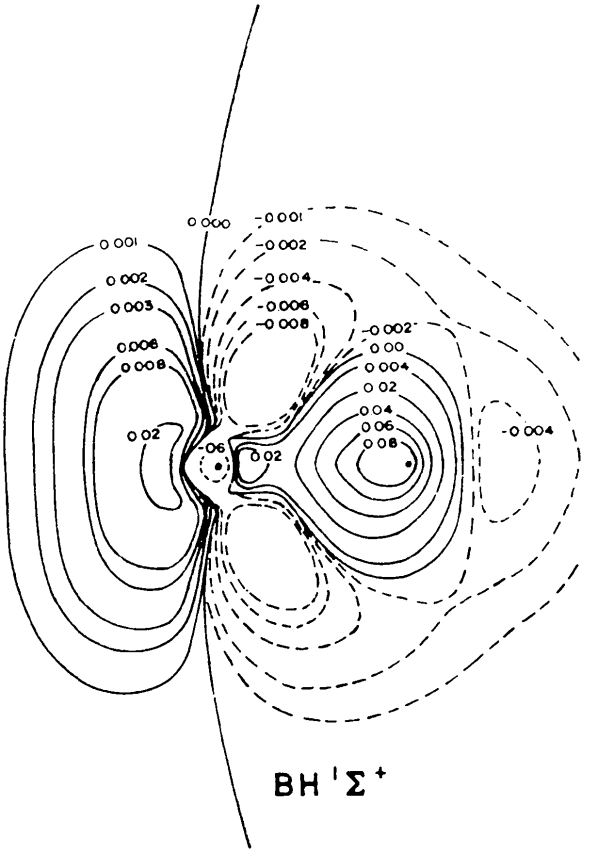

Fig. 11. Theoretical $M-A$ section along the B–H axis of the radical B–H. After Bader, Keaveny & Cade (1967). Contours are in a.u. and have to be multiplied by 6·7 to obtain e Å^{-3}.

about 0·4 Å apart from the proton. This corresponds closely to the distance of 0·45 Å in our $M - A$ maps. The peak height of 0·34 e Å^{-3} is about 60% of that in our $M - A$ curve. This is not surprising since LSL's calculations are based on a minimum basis set. It is well known and mentioned in LSL's paper that, with a minimum basis set, the charge density in bonding regions is underestimated.

For the three-centre bond (hydrogen bridge) B(1)–H(6)–B(3) (Fig. 6) our result differs from LSL's: our peak is four times as high as LSL's, and the shape of the peak is almost triangular in LSL's map whereas it is almost circular in ours. Our results seem to suggest closed three-centre bonds for the B–H–B bridges. But, in agreement with LSL's calculations, little excess charge is found along the B–B edges. LSL consider this to be an essential criterion for open three-centre bonds. It seems more likely to us, however, that the bond represents some intermediate state.

For the two-centre bond B(2)–B(3) (Fig. 7) there are differences in height, shape and position of the bond peak. In LSL's map the peak is very elongated perpendicular to the line B(2)–B(3) and obviously does not rise much above the 0·1 e Å^{-3} contour, while in our $M - A$ section it reaches more than 0·45 e Å^{-3} and concentrates much more on the line B(2)–B(3). In LSL's map the peak is located nearly midway between atoms B(2) and B(3), about 0·78 Å away from B(3), whereas in our map its distance from B(3) is only 0·66 Å. A shift of the peak to where it appears in the SCF calculation would certainly introduce systematic deviations in the corresponding $F_o - F_c$ sections.

Rather good agreement between LSL's and our sections is found for the remaining part of the boron framework. In the triangle B(5)–B(2)–B(5′) (Fig. 7) Lipscomb's theory predicts a closed three-centre bond. An increase of $M - A$ density between the atoms B(4) and B(1′), or their equivalent B(1)–B(4′), (Fig. 8) is found by us as well as by LSL. Good agreement is also observed in the triangle B(2′)–B(5)–B(1′), or its equivalent B(2)–B(5′)–B(1) (Fig. 8).

Generally, in our $M - A$ sections the positive contours appear to predominate whereas in LSL's sections the negative contours predominate. However, in both cases the sum over all difference densities should be zero. We conclude from this the following. Predominance of positive contours can also be observed in $X - N$ maps. The negative density is mostly spread far from the atoms and has little pronounced structure so that its minima rarely surpass the −0·05 e Å^{-3} contour. This is a consequence of the scattering factors used for the neutral atoms: they correspond to a rather diffuse density distribution of the outer-shell electrons. On the other hand, predominance of negative contours in LSL's maps arises because a minimum basis was used. Extended bases produce more positive contours in the bonding regions. An instructive example is given by Laws, Stevens & Lipscomb's (1972*b*) paper on diborane, where a direct comparison of difference maps for various basis sets is made.

Next, we compared the localized two-centre bonds in the terminal B–H groups (Fig. 4) with the corresponding section for the B–H radical as calculated by Bader, Keaveny & Cade (1967) (Fig. 11). This calculation is based on an extended basis and certainly gives a precise picture of the charge distribution in the radical. Although the situation at the B atom is quite different from that at the B atoms in decaborane, the bond in the radical must be a localized σ bond too.

The main difference in the two cases should be confined to the polarization of the bonds. The cusps of the density at the B nuclei cannot be observed in the experimental $M - A$ maps. But the heights (of about 0·55 e Å^{-3}) and the half-height widths (of approximately 0·8 Å) of the diffuse peaks in the bonding regions of the terminal B–H bonds in decaborane agree well with the corresponding values, ~0·6 e Å^{-3} and ~0·7 Å, respectively, in the B–H radical (Fig. 11). Moreover, the diffuse peaks in our $M - A$ maps also show an elongation towards the B atoms, though not as pronounced as in Fig. 11. On the other hand, in the radical the peak in the bonding region is much closer to the proton (about 13σ) (*i.e.* at a distance of about 0·14 Å) than that found for the B–H bonds in decaborane (0·45 Å). As, however, the peak height and shape are found to be similar, the amount of excess charge should be roughly the same in the two types of bonds. This suggests that the H atoms in decaborane are more positive than the one in the B–H radical.

Finally, the molecular dipole moment is related to the molecular charge distribution and may also serve for comparison. Bottei & Laubengayer (1962) have measured 3·17, 3·62 and 3·39 D, using solutions of decaborane in CS_2, C_6H_6 and C_6H_{12}, respectively. The SCF study of LSL gives 4·556 D, simple INDO and CNDO calculations yield 7·565 and 7·837 D respectively. Model I gives 3·03, models II and III give 6·02 and 6·67 D respectively. The latter values are too large, although in the crystal, a somewhat larger dipole moment can be expected than for isolated molecules or solutions. In the crystal the molecules form dipole chains along the twofold axes. This arrangement should induce an additional dipole moment in the molecules, which, however, will certainly not exceed 1 D.

Conclusion

With the type of models used in this paper, the true density distribution of a molecule can only be represented approximately, but the models are advantageous in that they can be easily formulated and well adapted to the needs of structure determination. Local chemical symmetry can easily be taken into account because the parameters are defined in the Cartesian coordinate system of a bond. Similarly, it is possible to exploit the

chemical equivalence of different parts of the molecule by reducing the number of parameters by means of constraints.

As density details in the vicinity of the nuclei cannot be observed by diffraction methods, a theoretical approximation for the atomic cores is important. With the use of scattering factors, based on the L-shell projection method with a Hartree–Fock basis, only one parameter need be employed for an atomic core and, at the same time, a fairly good description of the core density is achieved. Thus, the parameters introduced are mainly used to describe the excess density. Since shape parameters can generally be determined with less accuracy than positional parameters, the excess density is represented by a superposition of Gaussian distributions, whose positional parameters could be well determined. The advantages of empirical models are also pointed out by Hirshfeld (1971). The elimination of the thermal smearing from our models is very simple, and the resulting $M-A$ synthesis facilitates the comparison with quantum-chemical results.

The F_o-F_c syntheses show that the refinements with the given data were complete. The estimated standard deviation in the final difference maps is about 0·05 e Å^{-3}. The errors in the static $M-A$ maps are probably of the same order, but, because of twofold and fourfold symmetry, are reduced by factors of 0·71 and 0·50 respectively. On the other hand, series termination has lowered the terminal B–H bond peaks in the $M-A$ maps by about 0·1 to 0·2 e Å^{-3}. The density distribution at the nuclear cusps was not (and cannot be) the subject of our experimental investigation.

On the other hand, the featureless F_o-F_c syntheses show that our attempt to account for the diffuse peaks in the $X-N$ maps by means of a model for the molecular density distribution was successful as a whole. We do not claim that the two models used in this work are the only ones possible in order to obtain good agreement with the X-ray data, but we believe that no better agreement can be reached with other models. Hence, we argue that the density distributions, presented in the $M-A$ maps, are about as accurate as they can be, with the X-ray data and the neutron parameters used in this investigation.

Fair agreement is reached with quantum-chemically calculated density sections for the decaborane molecule (LSL). As a rule, the peaks in our $M-A$ maps are higher. It is well known that, with a limited basis, quantum-chemical calculations yield bond peaks which are too low. Therefore, we believe that the higher peaks in our $M-A$ maps are closer to the real density distribution in the decaborane molecule than those calculated by LSL. This is supported by the fact that the terminal B–H bond peaks in our $M-A$ maps agree in height and shape with the accurately calculated bond peak in the B–H radical (Bader, Keaveny & Cade, 1967).

We thank the Deutsche Forschungsgemeinschaft for support of this work.

References

BADER, R. F. W., KEAVENY, I. & CADE, P. E. (1967). *J. Chem. Phys.* **47**, 3381–3402.

BOTTEI, R. S. & LAUBENGAYER, A. W. (1962). *J. Phys. Chem.* **66**, 1449–1451.

BRILL, R., DIETRICH, H. & DIERKS, H. (1971). *Acta Cryst.* B**27**, 2003–2018.

BUSING, W. R. (1971). *Acta Cryst.* A**27**, 683–684.

DIERKS, H. & DIETRICH, H. (1968). *Z. Kristallogr.* **128**, 259–272.

DIETRICH, H. (1976*a*). *Acta Cryst.* A**32**, 347–348.

DIETRICH, H. (1976*b*). *J. Appl. Cryst.* **9**, 238–239.

HIRSHFELD, F. L. (1971). *Acta Cryst.* B**27**, 769–781.

International Tables for X-ray Crystallography (1962). Vol. III. Birmingham: Kynoch Press.

LAWS, E. A., STEVENS, R. M. & LIPSCOMB, W. N. (1972*a*). *J. Am. Chem. Soc.* **94**, 4467–4474.

LAWS, E. A., STEVENS, R. M. & LIPSCOMB, W. N. (1972*b*). *J. Am. Chem. Soc.* **94**, 4461–4467.

PAWLEY, G. S. (1972). *Adv. Struct. Res. Diffr. Methods*, **4**, 1–64.

RAYMOND, K. N. (1972). *Acta Cryst.* A**28**, 163–166.

REES, B. (1976). *Acta Cryst.* A**32**, 483–488.

SCHERINGER, C. (1965*a*). *Acta Cryst.* **19**, 504–513.

SCHERINGER, C. (1965*b*). *Acta Cryst.* **19**, 513–524.

SCHERINGER, C. (1977*a*). *Acta Cryst.* A**33**, 426–429.

SCHERINGER, C. (1977*b*). *Acta Cryst.* A**33**, 430–433.

SCHERINGER, C. (1977*c*). *Acta Cryst.* A**33**, 588–592.

STEWART, R. F. (1970). *J. Chem. Phys.* **53**, 205–213.

TIPPE, A. & HAMILTON, W. C. (1969). *Inorg. Chem.* **8**, 464–470.